Including Anatomical and Functional Information in MC Simulation of PET and SPECT Brain Studies. *Brain-VISET*: A Voxel-Based Iterative Method

Berta Marti-Fuster*, Oscar Esteban, Kris Thielemans, Xavier Setoain, Andres Santos, Domenec Ros, and Javier Pavia

***Abstract*—Monte Carlo (MC) simulation provides a flexible and robust framework to efficiently evaluate and optimize image processing methods in emission tomography. In this work we present *Brain-VISET* (Voxel-based Iterative Simulation for Emission Tomography), a method that aims to simulate realistic [^{99m}Tc]-SPECT and [^{18}F]-PET brain databases by including anatomical and functional information. To this end, activity and attenuation maps generated using high-resolution anatomical images from patients were used as input maps in a MC projector to simulate SPECT or PET sinograms. The reconstructed images were compared with the corresponding real SPECT or PET studies in an iterative process where the activity inputs maps were being modified at each iteration. Datasets of 30 refractory epileptic patients were used to assess the new method. Each set consisted of structural images (MRI and CT) and functional studies (SPECT and PET), thereby allowing the inclusion of anatomical and functional variability in the simulation input models. SPECT and PET sinograms were obtained using the SimSET package and were reconstructed with the same protocols as those employed for the clinical studies. The convergence of *Brain-VISET* was evaluated by studying the behavior throughout iterations of the correlation coefficient, the quotient image histogram and a ROI analysis comparing simulated with real studies. The realism of generated maps was also evaluated. Our findings show that *Brain-VISET* is able to generate realistic SPECT and PET studies and that four iterations is a suitable number of iterations to guarantee a good agreement between simulated and real studies.**

***Index Terms*—Anatomical variability, emission tomography, epilepsy, functional variability, Monte Carlo (MC) simulation.**

I. Introduction

MONTE CARLO (MC) simulation is a valuable tool in the assessment and optimization of image processing methods in emission tomography [1]. Although using real studies from subjects or phantoms has its benefits, MC simulation provides a flexible environment where the ground truth is known and where the realism of the input models and the equipment can be suitably reproduced. Hence, the number of scientific papers related to MC simulation has seen a considerable increase since the early 1990s [2].

In neuroimaging, MC simulation has been applied in several fields such as the evaluation of reconstruction methods [3], [4], statistical toolkits [5], [6], quantification methods [7]–[9], registration algorithms [10]–[12], segmentation methods [13]–[16], among others. The more realistic the simulations, the more robust the assessment, and some attempts to include information from real data have been reported. Some authors include the anatomical information in the input models from brain magnetic resonance imaging (MRI) images [5], [17]. In order to obtain more realistic simulations, functional information has also been considered. Thus, Grova *et al.* [18] included the physiological variability from an inter-individual analysis of anatomically standardized SPECT data. In fields other than neuroimaging, several authors derive this information directly from real functional data of patients or healthy subjects [19]–[23]. However, to the best of our knowledge, the inclusion of functional and anatomical information from real patients in a voxel-by-voxel approach has not been considered. By using the information of each of the smallest elements of an image, the realism of the simulated data could possibly be improved.

The aim of this work was to develop and assess *Brain-VISET* (Voxel-based Iterative Simulation for Emission Tomography), a method for simulating comprehensive databases of realistic SPECT and PET studies which include anatomical and functional information. *Brain-VISET* uses high-resolution images (MRI and CT) to generate attenuation and initial activity maps.

Manuscript received April 08, 2014; revised May 06, 2014; accepted May 17, 2014. Date of publication May 22, 2014; date of current version September 29, 2014. This work was supported in part by Multimodal Imaging tools for Neurological Diseases (MIND-t) project of Biomedical Research Networking center in Bioengineering, Biomaterials and Nanomedicine (CIBER-BBN), in part by Spain's Ministry of Science and Innovation through SAF2009-08076, TEC2011-28972-C02-02, IPT-300000-2010-003 and CDTI-CENIT (AMIT project), and in part by Fondo de Investigaciones Sanitarias (PI12-00390). *Asterisk indicates corresponding author.*

*B. Marti Fuster is with the Biophysics and Bioengineering Unit, Physiological Sciences Department I, School of Medicine, University of Barcelona, 08036 Barcelona, Spain, and also with Biomedical Research Networking Center, Bioengineering, Biomaterials and Nanomedicine (CIBER-BBN)-Spain, 08036 Barcelona, Spain.

D. Ros is with the Biophysics and Bioengineering Unit, Physiological Sciences Department I, School of Medicine, University of Barcelona-IDIBAPS, 08036 Barcelona, Spain, and also with the Biomedical Research Networking Center, Bioengineering, Biomaterials and Nanomedicine (CIBER-BBN)-Spain, 08036 Barcelona, Spain.

O. Esteban and A. Santos are with Biomedical Image Technologies, Departamento de Ing. Electrónica, ETSI Telecomunicación, Universidad Politécnica de Madrid, 28040. Madrid, Spain, and also with Biomedical Research Networking Center, Bioengineering, Biomaterials and Nanomedicine (CIBER-BBN)-Spain, 28040 Madrid, Spain.

K. Thielemans is with the Institute of Nuclear Medicine, University College London, NW1 2BU London, U.K.

X. Setoain and J. Pavia are with Servei de Medicina Nuclear, Hospital Clínic, IDIBAPS, 08036 Barcelona, Spain, and also with Biomedical Research Networking center in Bioengineering, Biomaterials and Nanomedicine (CIBER-BBN)-Spain, 08036 Barcelona, Spain.

Digital Object Identifier 10.1109/TMI.2014.2326041

The activity map is modified using an iterative voxel-by-voxel approach with functional information obtained from a real SPECT or PET study. The method was used to simulate realistic studies in refractory epilepsy. For the *Brain-VISET* validation, the agreement between real and simulated studies was assessed. The realism of the generated input maps was also evaluated.

II. Materials and Methods

A. Population of Subjects, Data Acquisition, and Preprocessing

Simulation datasets were based on the brain scans of 30 drug-resistant epileptic patients selected from the pre-surgical epilepsy database at the Hospital Clínic of Barcelona, Spain. As part of the pre-surgical evaluation in epilepsy, all patients underwent preoperative localization of the epileptogenic focus using video-EEG monitoring, MRI, PET-CT and an interictal SPECT studies. All subjects gave written informed consent before entering the pre-surgical evaluation of the Epilepsy Unit.

MRI. High-resolution, 3-D T1-weighted images were acquired using a Siemens Tim Trio 3T in the sagittal plane with a matrix size of $224 \times 240 \times 256$ voxels ($0.86 \times 0.90 \times 0.86$ mm^3 voxel size) completely covering the brain.

Interictal PET-CT. PET-CT scans were performed using a hybrid PET/CT (Classic BIOGRAPH, SIEMENS, Knoxville, TN, USA) equipped with an ECAT EXACT HR+ BGO (Bismuth Germanium Oxide) PET scanner. PET images were acquired 60 min after intravenous injection of approximately 5 MBq/Kg of [^{18}F]-FDG in 3-D mode. The PET-CT scan time was 11 min, 1 min, for transmission, and 10 more for emission. Sixty three attenuation-corrected brain slices were obtained using the Ordered Subsets Expectation Maximization (OSEM) algorithm (16 subsets—six iterations) with a matrix of $128 \times 128 \times 63$ and $2.6 \times 2.6 \times 2.4$ mm^3 voxel size. The acquired CT scan, $512 \times 512 \times 64$ grid of $0.98 \times 0.98 \times 2.4$ mm^3 voxel size, was already registered to the PET study.

Interictal SPECT. SPECT studies were acquired after injection of [^{99m}Tc]- HMPAO (925 MBq), using an Infinia Hawkeye 4 (GE Healthcare) dual-head SPECT imaging system equipped with low-energy high-resolution (LEHR) parallel-hole collimators. The radius of rotation was 14 cm and 120 projections (128×128 matrix and 3.3×3.3 mm^2 pixel size) were acquired over 360° at 40 s/projection. Images were reconstructed using the filtered back projection (FBP) algorithm with a Butterworth filter of 0.42 cm^{-1} cut-off frequency and order 5.8.

MRI space of each patient was taken as the reference space. Thus, the PET, CT, and SPECT images of each patient were registered to the MRI. Emission tomography studies were registered to MRI using the registration algorithms of *FocusDET* [24]. The CT scan was registered to the MRI by using the transformation matrix obtained in the PET-MRI registration. Each registration was visually validated and manually corrected when necessary.

B. Brain-VISET

Fig. 1 shows a flowchart of the iterative simulation method proposed. The flowchart is divided into two steps. The first (lighter dashed box) includes the anatomical information from an MRI and a CT image to obtain a simulated SPECT or PET study. This step is performed only once. In step 2 (heavier dashed box), the reconstruction obtained in step 1 is compared voxel-by-voxel with the clinical SPECT or PET data in order to modify the activity model used in the simulation. This step can be repeated until the simulated and clinical studies are similar enough. The details involved in these two steps as well as an evaluation of the new method are set out below.

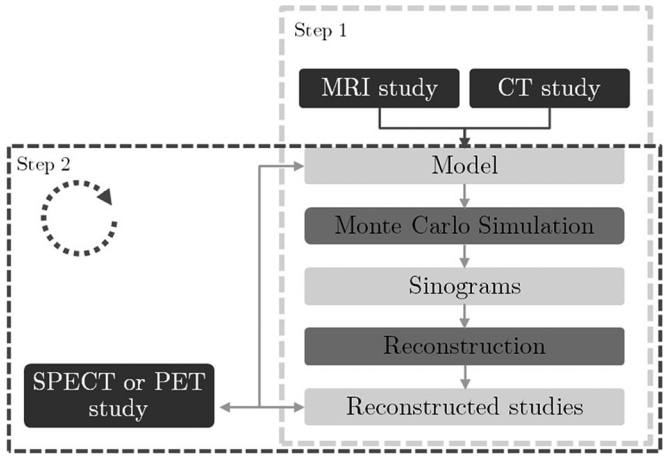

Fig. 1. Flowchart of *Brain-VISET*.

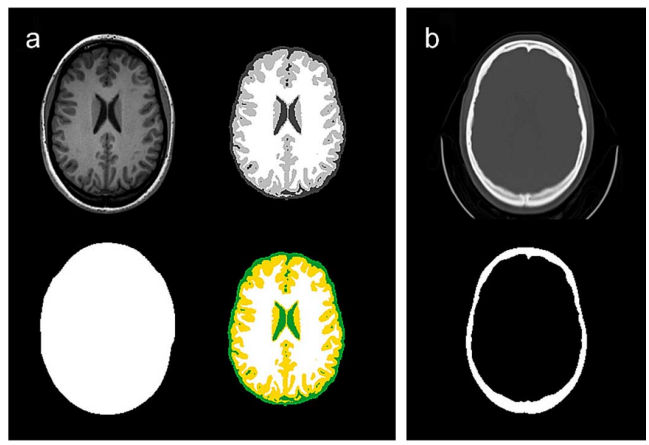

Fig. 2. Generation of initial maps. a: From left to right and top to bottom, T1-weighted MRI, extracted brain image, outskin image, and its corresponding brain tissue segmentation. b: CT (top) and bone (bottom) images.

1) Including the Anatomical Information (Step 1): MC simulations of brain SPECT or PET data require an activity map of radiotracer distribution and an attenuation map describing the attenuation coefficients of the head. In our study, T1-weighted MRI and CT data were used to generate the initial maps. T1-weighted MRI studies were brain-extracted using BET [25] and segmented with FAST [26] (both tools included in FSL [27]) to obtain the image set presented in Fig. 2(a), from left to right and top to bottom: 1) T1-weighted MRI, 2) extracted brain image, 3) outskin image, and 4) brain tissue segmented image (grey matter, white matter and cerebrospinal fluid (CSF) separately). Bone tissue was extracted from the CT image by thresholding [see Fig. 2(b)]. Hounsfield values greater than 600 were considered to be bone.

The attenuation maps were generated from a combination of the bone tissue and outskin images. Two attenuation media were distinguished: 1) bone ($\mu_{\mathrm{SPECT}} = 0.323$ cm^{-1} and $\mu_{\mathrm{PET}} = 0.196$ cm^{-1}) and 2) all other tissues, i.e., everything inside the head other than bone ($\mu_{\mathrm{SPECT}} = 0.155$ cm^{-1} and $\mu_{\mathrm{PET}} = 0.098$ cm^{-1}). To generate the activity maps, information from all images in Fig. 2 was taken into account. Four tissue types were defined in the initial activity map, based on empirical measures. Grey matter was considered to be the tissue of highest uptake and so was assigned a value of 100, white matter was given a value of 25, CSF and everything that is neither bone nor brain received a value of 4 for SPECT simulations and 20 for PET simulations, and finally, bone had a value of 0.

SimSET v2.9 MC code [28] was employed to simulate SPECT and PET sinograms. In SPECT simulation the Infinia Hawkeye 4 from GE Healthcare was modeled to generate emission projections using ^{99m}Tc as the radioisotope. The simulated collimator had hexagonal holes (radius: 0.75 mm, septal thickness: 0.2 mm) and 35 mm in length. One hundred twenty projections over 360° (matrix size: 128×54, pixel size: 3.3×3.3 mm^2) were simulated, using a 20% energy window centered on 140 keV. In PET simulation, a BGO-based Siemens Biograph scanner was modeled to generate emission and transmission projections using ^{18}F as the radioisotope. Random events and dead-time were not modeled during the simulations. A cylindrical detector of 32 axial rings of 41.2 cm radius was simulated. A 3-D-mode acquisition with no axial compression (maximum ring difference of 31 and span one) was simulated using an energy window of 350–650 keV. Sinogram dimensions were 288 transaxial bins (bin size: 2.2 mm) and 288 angular positions. In PET simulations, photons were separated into true and scatter coincidences, allowing us an ideal scatter correction because only the true photons were considered in the reconstruction. Simulations were performed in order to obtain sinograms with 5 million counts in SPECT projections and around 80 million counts in PET simulations.

Simulated studies were reconstructed in a similar way to the clinical data. Thus, SPECT reconstruction was performed using FBP and a Butterworth filter with 0.42 cm^{-1} cut-off frequency and order 5.8. PET sinograms were firstly corrected for attenuation using SimSET tools. Then, the sinograms were combined with axial compression (span nine) and reconstructed by using an OSEM-based algorithm (eight subsets, 12 iterations), both processes being performed with the STIR package [29]. Before reconstruction, the sinograms were normalized using normalization factors previously calculated, rebinning a uniform sinogram (all values set to one).

2) Including the Functional Information (Step 2): The activity maps were updated by incorporating the functional information provided by the clinical studies

$$M_i^{k+1} = M_i^k \cdot C_i / S_i^k \quad S_i^k > 0 \tag{1}$$

where M_i^k is the value of the activity map in voxel i at iteration k, M_i^{k+1} is the corresponding updated value, C_i is the value of the clinical study in voxel i and S_i^k is the value of the simulated study in voxel i at iteration k. Bone and outskin information was used to ensure that the updated activity map (M_i^{k+1}) is zero in those voxels belonging to tissues where there is no radiotracer uptake. Simulation and reconstruction processes for SPECT and PET data were performed as per step 1.

3) Assessment of Generated Studies: To evaluate the similitude between the simulated and real images, the correlation coefficient (CC) and the histogram of quotient image (C_i/S_i^k) were calculated. A theoretical value of 1 for CC and a Dirac delta distribution for the quotient image histogram should be obtained when the two images have identical distribution. Thus, studying the behavior of these functions throughout the iterative process we could: 1) assess the convergence of the method and 2) define the stopping criterion by determining the number of iterations necessary to ensure a good agreement between images.

The *Brain-VISET* method was assessed for both modalities, PET and SPECT, by using 30 studies of our dataset, calculating CC and quotient image histograms for 1–10 iterations.

A region of interest (ROI) analysis was also performed for different brain structures by comparing activity concentrations between real and simulated studies in a digital human brain atlas [30]. To this end, the contrast (Con) was calculated. This parameter was defined as the ratio between the mean activity in a selected ROI and the mean activity in a reference region covering the whole white matter region. A bias between contrasts obtained from clinical and simulated data for each subject j and for each ROI i was calculated as

$$b_{ij}^k = \frac{\mathrm{Con\_}S_{ij}^k - Con\_C_{ij}}{\mathrm{Con\_}C_{ij}} \times 100 \tag{2}$$

where Con_C_{ij} is the contrast at ROI i of subject j of the clinical data and $Con\_S_{ij}^k$ is the contrast at ROI i of subject j of the simulated study at iteration k. Then, mean biases and standard deviations for each iteration of the *Brain-VISET* method were calculated for each ROI over the 30 (N) studies as

$$b_i^k = \frac{1}{N} \sum_j b_{ij}^k \tag{3}$$

$$\sigma_i^k = \sqrt{\frac{1}{N} \sum_j \left(b_{ij}^k - b_i^k\right)^2}. \tag{4}$$

Finally, in order to assess the behavior of ROI analysis throughout iterations, a global mean bias and a global standard deviation over the 110 (M) ROIs were calculated as

$$b^k = \frac{1}{M} \sum_i b_i^k \tag{5}$$

$$\sigma^k = \sqrt{\frac{1}{MN} \sum_i \sum_j \left(b_{ij}^k - b^k\right)^2}. \tag{6}$$

All studies of SPECT and PET from our dataset (N = 30) were used for the ROI analysis. This was performed in the Montreal Neurological Institute (MNI) standard space where the ROI atlas is defined. SPECT and PET studies were normalized to the standard space using the MRI deformation fields. These fields described the spatial deformations to normalize each individual MRI to MNI space and were obtained by

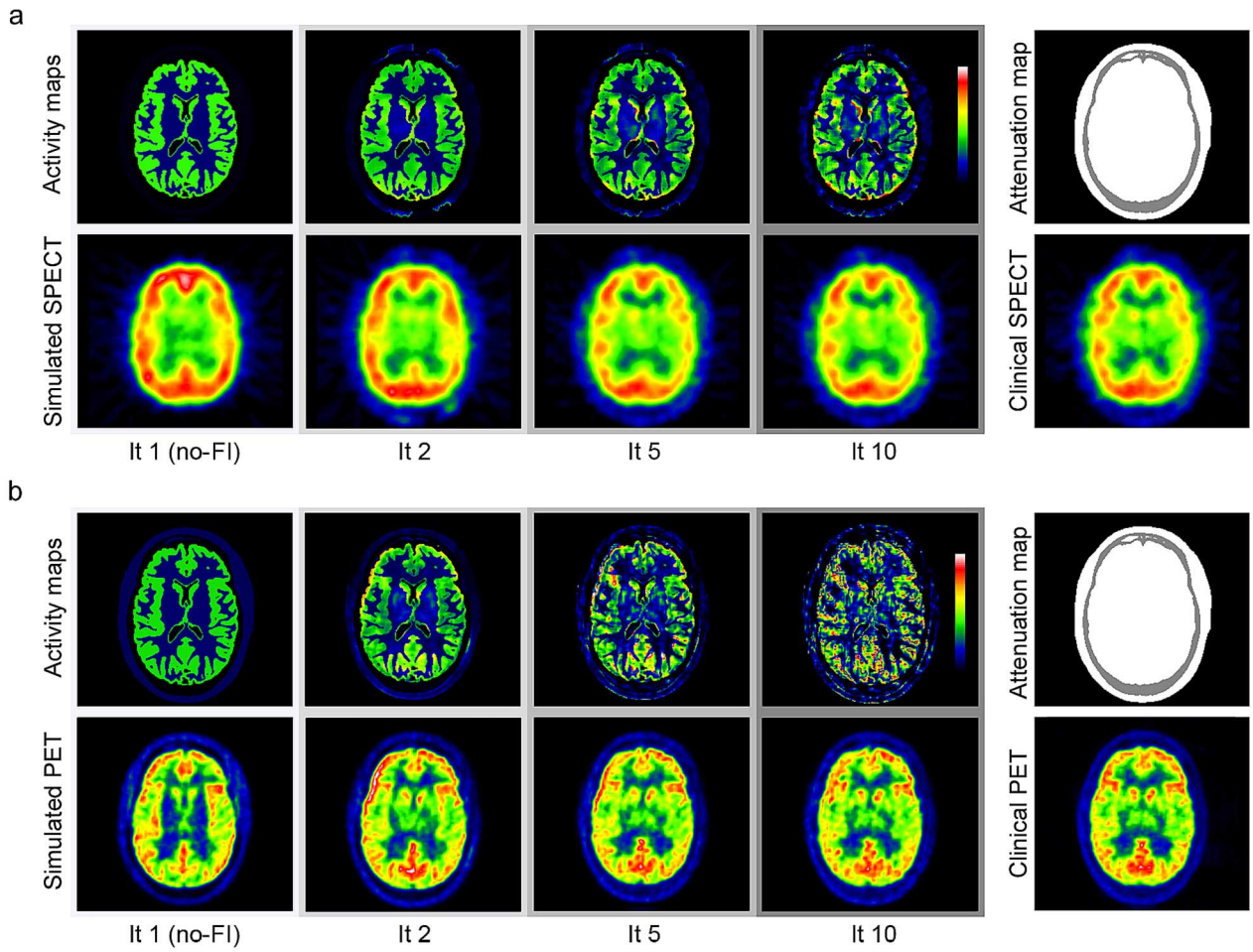

Fig. 3. *Brain-VISET* results for SPECT (a) and PET (b) studies. Upper row: activity maps at iterations one, two, five, and 10 and attenuation map. Bottom row: simulated images and clinical study.

normalizing each MRI study using the DARTEL method, an alternative normalization method in SPM8 [31].

4) Assessment of Generated Models: In addition to the assessment of generated studies, the realism of the generated models was also evaluated. For this purpose, the clinical SPECT or PET study from Fig. 1 was replaced by a simulated study where the input model was known. Thus, we used the previously simulated studies at iteration five (S^5) as the "clinical" study in Fig. 1 and the corresponding model as the theoretical activity map (M^5). Then, the activity maps (M'^k) generated throughout *Brain-VISET* iterations were compared with the theoretical M^5.

CC and the ROI analysis described in the subsection above were also performed to quantify the realism of generated models for 1 to 10 iterations using the 30 studies from our dataset.

III. Results

A. Brain-VISET

1) Simulated Studies: Simulated studies were obtained using an Intel Core i7 CPU 3.7 GHz 12 GB of RAM system. Mean computational time to perform a SPECT iteration was 5 h, consuming a maximum of 0.5 GB of RAM, whereas for a PET iteration the time was 24 h on average, consuming a maximum of 2.7 GB of RAM. In order to speed up PET simulations and taking advantage of the fact that SimSET simulation is intrinsically parallelizable, a different simulation strategy was followed for PET. By parallelizing PET simulation into eight simultaneous processes, the mean time was reduced to 3 h per iteration.

Fig. 3 shows examples of MC simulation of SPECT (a) and PET (b) studies using *Brain-VISET*. Pairs of activity maps and simulated studies are shown for both modalities. The corresponding clinical study is shown on the right side of Fig. 3(a) and (b), below the attenuation map. It can be seen that as the iteration number increases, the simulated images become more similar to the clinical studies. Note that the simulated images at the first iteration correspond to those obtained in the first step of the method, when no functional information is included. Throughout the paper, FI or no-FI abbreviations will be used to indicate whether the functional information was included or not.

2) Assessment of Generated Studies: Fig. 4 shows the CC between clinical and simulated studies against the iteration number. CC rapidly increases during the first iterations and reaches a plateau after four iterations in both modalities.

Fig. 5 shows an example of the quotient image histograms between the simulated and clinical studies for SPECT (a) and

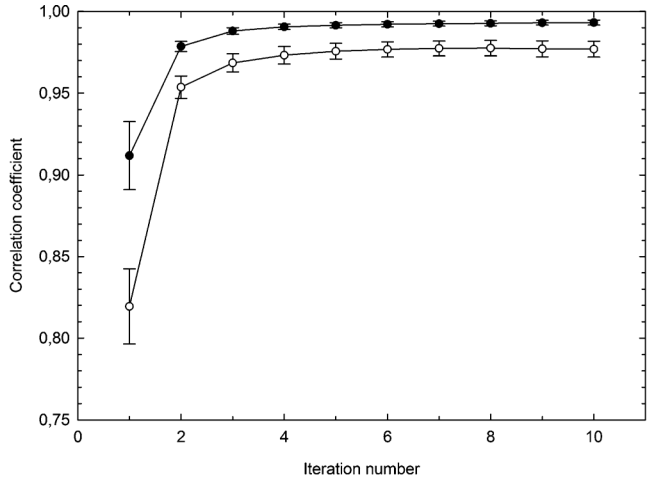

Fig. 4. CC between simulated and clinical data for SPECT (filled circles) and PET (hollow circles) studies as function of the iteration number.

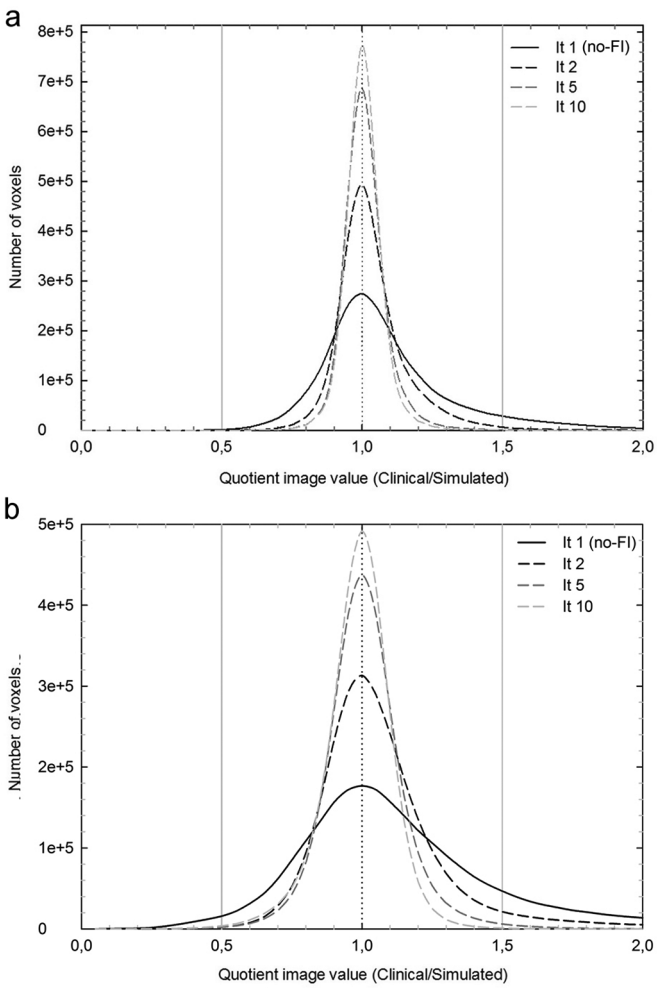

Fig. 5. Histograms of the quotient images between clinical and simulated SPECT (a) and PET (b) data. Solid line: histograms when no-FI was included in simulation. Dashed lines: histograms at iterations 2, 5, and 10 when FI was included in simulation. Vertical dotted line: Ideal value of quotient image. Vertical solid lines: lower and upper limits of the range values used to obtain statistic moments of the histogram.

PET (b) data. The solid line represents the quotient image histogram between clinical and no-FI simulated data, with

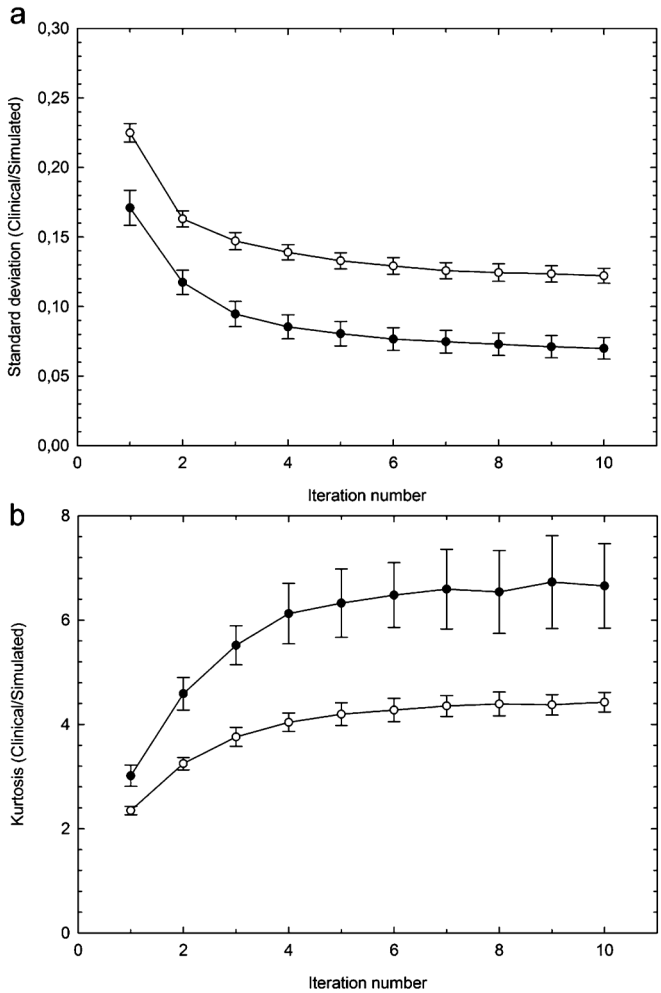

Fig. 6. Standard deviation (a) and kurtosis (b) of the quotient image histogram values for SPECT (filled circles) and PET (hollow circles) studies.

dashed lines indicating the quotient image histogram between clinical and FI simulated data at iterations two, five and ten. A dotted vertical line shows the ideal value of these quotients $(= 1)$, when no differences exist between simulated and real data. It can be seen that distributions become taller and thinner as iterations increase. In order to quantitatively assess this behavior, standard deviation, and kurtosis (as a measure of peakedness) were calculated. Solid vertical lines indicate the limits of the quotient image values that were considered to obtain these parameters.

Fig. 6(a) and (b) shows the standard deviation and kurtosis against the iteration number. As in CC behavior, these parameters rapidly change with early iterations and tend to stabilize as the number of iterations increases.

The results of the ROI analysis are shown in Fig. 7(a) and (b) for SPECT and PET, respectively. In SPECT data, global bias is almost zero over the iterations, whereas in PET data the bias decreases, reaching a value close to zero $(< 2\%)$ when FI is included. On the other hand, global standard deviation of the bias in the ROIs (indicated as error bars) strongly decreases throughout iterations, remaining constant after four iterations in both modalities. It should be noted

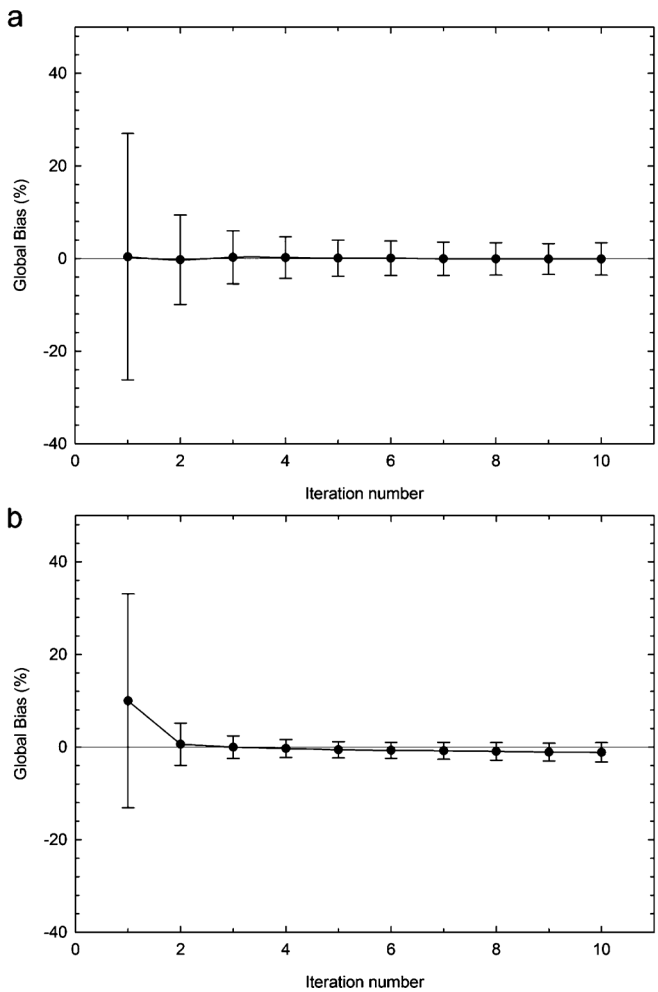

Fig. 7. SPECT (a) and PET (b) ROI global bias. Grey solid line is the ideal value of the bias (0).

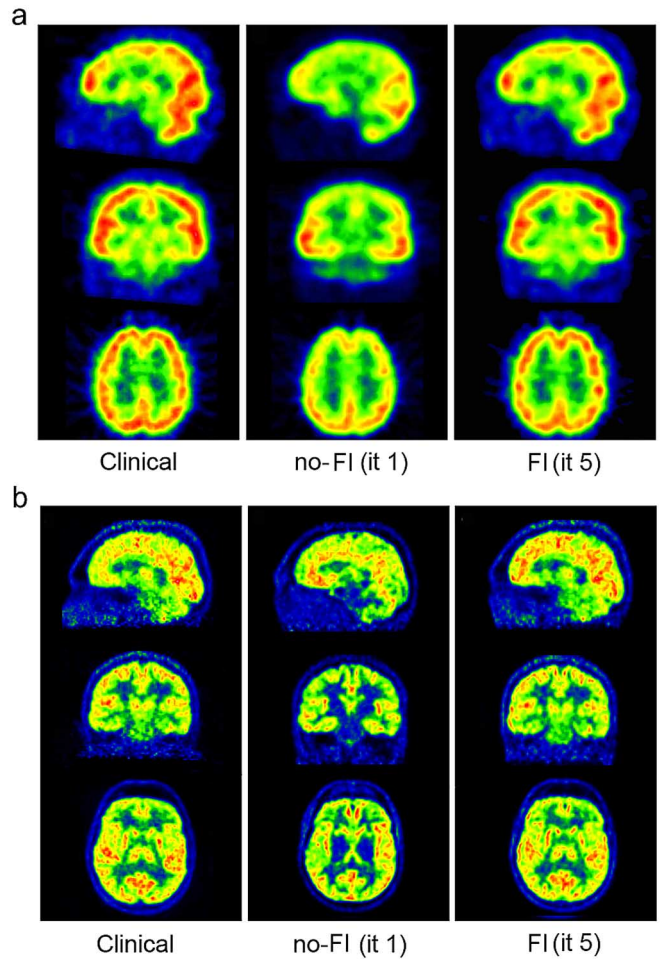

Fig. 8. Sagittal, coronal and axial views of SPECT (a) and PET (b) studies. From left to right: clinical image, no-FI simulated image (it 1) and FI simulated image (it 5).

that the dispersion of SPECT studies is higher than that of PET studies. This could be explained by the fact that PET studies always have greater number of counts (usually ten times greater) than SPECT studies.

Finally, Fig. 8 shows an example of SPECT (a) and PET (b) images obtained using *Brain-VISET*. In both images, the first column shows sagittal, coronal and axial views of the clinical study, and the second and third columns show the same views of the no-FI and FI (it 5) simulated data.

3) Assessment of Generated Models: Fig. 9 shows the CC between each new generated map (M'^k) and the theoretical activity map (M^5) throughout *Brain-VISET* iterations. In this case, CC rapidly increases between the first and second iteration, remains almost constant in the next two iterations and finally, decreases slowly. This behavior is similar in both modalities although a more pronounced decrease is observed in PET studies (hollow circles).

The ROI analysis for the activity maps is shown in Fig. 10(a) and (b) for SPECT and PET, respectively. As for the generated studies (Fig. 7), the behavior of the mean global bias through iterations is quite similar and remains close to zero once FI is included. Global standard deviation (error bars) also decreases rapidly, reaching a constant value after four iterations.

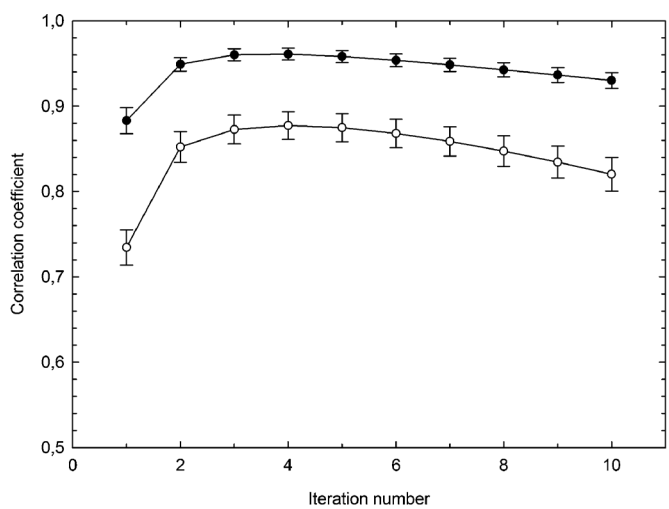

Fig. 9. CC between theoretical (M^5) and generated activity maps (M'^k) for SPECT (filled circles) and PET (hollow circles) studies as a function of the iteration number.

However, this dispersion is greater than that in the generated studies.

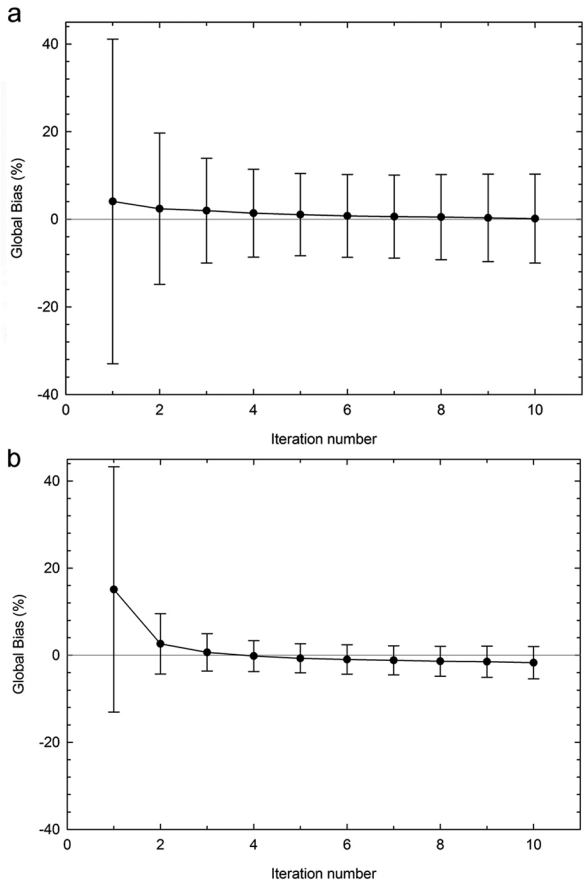

Fig. 10. SPECT (a) and PET (b) ROI global bias between activity maps. Grey solid line is the ideal value of the bias (0).

IV. Discussion

In the present study *Brain-VISET* has been developed and evaluated. This method is a voxel-based iterative approach which includes anatomical and functional information from clinical data in high-resolution input maps as suggested in an earlier study [32]. Although a simulated study will hardly recover all high-frequency details because of the digitization of the activity map, high-resolution input maps allow the simulated studies to achieve a spatial resolution similar to that observed in clinical studies.

Using *Brain-VISET*, the intrinsic heterogeneity between and within brain structures can be accurately modeled. This offers advantages over those methods that add the functional information into piece-wise activity maps by using constant values or measurements from real studies. Other authors include the functional information voxel-by-voxel using the SPECT or PET study from a real patient directly as the activity map [20], [32], [33]. The novelty in this work lies in the inclusion of both functional and anatomical information (from MRI and CT) in an iterative simulation process. The use of anatomical information in the *Brain-VISET* method seems to be important to achieve the accurate results obtained from regional comparisons between simulated and clinical studies (Fig. 7). Less accurate results were obtained when the *Brain-VISET* process started using a uniform activity map (without MRI-based information).

Our findings show that four or five iterations are suitable values to ensure that functional information is properly included whilst avoiding the increase of noise in the generated maps. As shown in Figs. 5 – 7, four iterations can be considered as an acceptable trade-off between realistic results in simulated studies and computational demand. As regards generated models, CC between the generated and theoretical maps (Fig. 9) decreases after four iterations. This behavior can be attributed to the effect of noise which can also be visually perceived in the activity maps at iteration 10 in Fig. 3. The noise in this figure also seems to have a greater effect in PET than in SPECT models, in agreement with the more pronounced decrease observed in Fig. 9 for PET maps.

Brain-VISET appears to work equally well on SPECT and PET when simulated and clinical studies are visually compared (see Fig. 3). However, as the statistical parameters indicate, simulated-clinical pairs are more similar in SPECT than in PET (see Figs. 5 –7). We hypothesized that this behavior might be due to: 1) SPECTs lower spatial resolution and 2) better SPECT modelization, which included a more accurate simulation and reconstruction to mimic clinical studies. To prove the first hypothesis, the PET studies were smoothed until a spatial resolution similar to that of SPECT studies was reached. This resulted in improved statistical parameters that were closer to those of SPECT. On the other hand, the process of mimicking our real studies was less complicated for SPECT than for PET data. Commercial PET scanners use closed source software, being more difficult to accurately reproduce some image processing steps such as degradation corrections, rebinning or reconstruction. For example, the scatter was corrected using the true scattered photons provided by the Monte Carlo simulator and not by the scatter correction method of the PET scanner. This could account for some of the differences between the clinical and simulated images observed in our results. To demonstrate that clinical SPECT studies were better reproduced, we used the studies obtained in the assessment of generated models (using a simulated study as "clinical" study) to perform CC and ROI analysis of the generated studies. Both analyses for PET data were improved with respect to previous figures [Fig. 4 and Fig. 7(b)] and were closer to SPECT results.

Accuracy and computational demand are correlated in MC simulation. GATE [34], one of the packages most widely used because of its accuracy, has the inconvenience of long execution times. In this work SimSET, a package with a lower computational burden, was used. Our previous experience led us to consider SimSET as a suitable code to obtain realistic SPECT and PET simulations. This assumption was confirmed by the findings, showing that *Brain-VISET* can be run in a reasonable computational time on standard computers used in biomedical image processing. To accelerate the *Brain-VISET* method, a combination of Monte Carlo and analytical simulations could be explored, using the analytical simulation for the first iterations and a Monte Carlo simulation for the last ones. The accuracy of this approach should be assessed.

The results of this study show that *Brain-VISET* is a reliable simulation method for the generation of brain emission tomography data that could not be distinguished from clinical images, thereby allowing the assessment of image processing methods in a realistic and well-controlled environment. The proposed methodology for including functional information might be extended to other emission tomography studies. Nonetheless, the difficulties derived from image processing of soft tissue, such as segmentation, respiratory motion correction or registration, need to be addressed.

Further work will be carried out to make freely available the generated database from our 30 drug-resistant epileptic patients and to create comprehensive databases from healthy subjects which could be easily modified to simulate pathologies.

V. Conclusion

This paper details the development and assessment of *Brain-VISET*, a voxel-based iterative method for realistic MC simulation of SPECT and PET studies. Applying *Brain-VISET* to image sets from 30 refractory epileptic patients, a comprehensive database was generated. After four iterations a good agreement was obtained between simulated and real studies.

References

[1] H. Zaidi, "Relevance of accurate Monte Carlo modeling in nuclear medical imaging," *Med. Phys.*, vol. 26, no. 4, pp. 574–608, 1999.

[2] I. Buvat and I. Castiglioni, "Monte Carlo simulations in SPET and PET," *Q. J. Nucl. Med.*, vol. 46, no. 1, pp. 48–61, 2002.

[3] A. Cot, C. Falcon, C. Crespo, J. Sempau, D. Pareto, S. Bullich, F. Lomena, F. Calvino, J. Pavia, and D. Ros, "Absolute quantification in dopaminergic neurotransmission SPECT using a Monte Carlo-based scatter correction and fully 3-dimensional reconstruction," *J. Nucl. Med.*, vol. 46, no. 9, pp. 1497–1504, 2005.

[4] J. Ouyang, G. E. Fakhri, and S. Moore, "Fast Monte Carlo based joint iterative reconstruction for simultaneous 99 mTc/123I SPECT imaging," *Med. Phys.*, vol. 34, no. 8, pp. 3263–3272, 2007.

[5] P. Aguiar, D. Pareto, J. D. Gispert, C. Crespo, C. Falcon, A. Cot, F. Lomena, J. Pavia, and D. Ros, "Effect of anatomical variability, reconstruction algorithms and scattered photons on the SPM output of brain PET studies," *NeuroImage*, vol. 39, no. 3, pp. 1121–1128, 2008.

[6] D. Pareto, P. Aguiar, J. Pavia, J. D. Gispert, A. Cot, C. Falcon, A. Benabarre, F. Lomena, E. Vieta, and D. Ros, "Assessment of SPM in perfusion brain SPECT studies. A numerical simulation study using bootstrap resampling methods," *IEEE Trans. Biomed. Eng.*, vol. 55, no. 7, pp. 1849–1853, Jul. 2008.

[7] M. Soret, P. Koulibaly, J. Darcourt, S. Hapdey, and I. Buvat, "Quantitative accuracy of dopaminergic neurotransmission imaging with (123)I SPECT," *J. Nucl. Med.*, vol. 44, no. 7, pp. 1184–1193, 2003.

[8] S. Hapdey, M. Soret, and I. Buvat, "Quantification in simultaneous (99m)Tc/(123)I brain SPECT using generalized spectral factor analysis: A Monte Carlo study," *Phys. Med. Biol.*, vol. 51, no. 23, pp. 6157–6171, 2006.

[9] C. Crespo, J. Gallego, A. Cot, C. Falcon, S. Bullich, D. Pareto, P. Aguiar, J. Sempau, F. Lomena, F. Calvino, J. Pavia, and D. Ros, "Quantification of dopaminergic neurotransmission SPECT studies with 123I-labelled radioligands. A comparison between different imaging systems and data acquisition protocols using Monte Carlo simulation," *Eur. J. Nucl. Med. Mol. Imag.*, vol. 35, no. 7, pp. 1334–1342, 2008.

[10] E. U. Mumcuoglu, F. Nar, Y. Yardimci, U. Kocak, E. L. Ergun, B. V. Salanci, O. Ugur, and B. Erbas, "Simultaneous surface registration of ictal and interictal SPECT and magnetic resonance images for epilepsy studies," *Nucl. Med. Commun.*, vol. 27, no. 1, pp. 45–55, 2006.

[11] L. Thurfjell, Y. H. Lau, J. L. Andersson, and B. F. Hutton, "Improved efficiency for MRI-SPET registration based on mutual information," *Eur. J. Nucl. Med.*, vol. 27, no. 7, pp. 847–856, 2000.

[12] B. Aubert-Broche, A. C. Evans, and L. Collins, "A new improved version of the realistic digital brain phantom," *NeuroImage*, vol. 32, no. 1, pp. 138–145, 2006.

[13] B. He and E. C. Frey, "The impact of 3-D volume of interest definition on accuracy and precision of activity estimation in quantitative SPECT and planar processing methods," *Phys. Med. Biol.*, vol. 55, no. 12, pp. 3535–3544, 2010.

[14] M. S. Sharif, M. Abbod, A. Amira, and H. Zaidi, "Artificial neural network-based system for PET volume segmentation," *Int. J. Biomed. Imag.*, vol. 2010, 2010.

[15] M. Pacilio, C. Basile, S. Shcherbinin, F. Caselli, G. Ventroni, D. Aragno, L. Mango, and E. Santini, "An innovative iterative thresholding algorithm for tumour segmentation and volumetric quantification on SPECT images: Monte Carlo-based methodology and validation," *Med. Phys.*, vol. 38, no. 6, pp. 3050–3061, 2011.

[16] M. Werner-Wasik, A. D. Nelson, W. Choi, Y. Arai, P. F. Faulhaber, P. Kang, F. D. Almeida, Y. Xiao, N. Ohri, K. D. Brockway, J. W. Piper, and A. S. Nelson, "What is the best way to contour lung tumors on PET scans? Multiobserver validation of a gradient-based method using a NSCLC digital PET phantom," *Int. J. Radiat Oncol. Biol. Phys.*, vol. 82, no. 3, pp. 1164–1171, 2012.

[17] B. Aubert-Broche, C. Grova, A. Reilhac, A. C. Evans, and D. L. Collins, "Realistic simulated MRI and SPECT databases. Application to SPECT/MRI registration evaluation," *Med. Image Comput. Comput. Assist. Interv.*, vol. 9, no. 1, pp. 330–337, 2006.

[18] C. Grova, P. Jannin, A. Biraben, I. Buvat, H. Benali, A. M. Bernard, J. M. Scarabin, and B. Gibaud, "A methodology for generating normal and pathological brain perfusion SPECT images for evaluation of MRI/SPECT fusion methods: Application in epilepsy," *Phys. Med. Biol.*, vol. 48, no. 24, pp. 4023–4043, 2003.

[19] I. Castiglioni, I. Buvat, G. Rizzo, M. Gilardi, J. Feuardent, and F. Fazio, "A publicly accessible Monte Carlo database for validation purposes in emission tomography," *Eur. J. Nucl. Med. Mol. Imag.*, vol. 32, no. 10, pp. 1234–1239, 2005.

[20] T. Carlier, P. Descourt, L. Maigne, D. Visvikis, and M. Bardies, "Efficient simulations of iodine 131 SPECT scans using gate," in *IEEE Nucl. Sci. Symp. Conf. Rec.*, 2009, pp. 3412–3414.

[21] A. L. Maitre, W. Segars, S. Marache, A. Reilhac, M. Hatt, S. T. S, C. Lartizien, and D. Visvikis, "Incorporating patient specific variability in the simulation of realistic whole body 18F-FDG distributions for oncology applications," *Proc. IEEE*, vol. 97, no. 12, pp. 2026–2038, Dec. 2009.

[22] S. Tomei, A. Reilhac, D. Visvikis, N. Boussion, C. Odet, F. Giammarile, and C. Lartizien, "OncoPET_DB: A freely distributed database of realistic simulated whole body 18F-FDG PET images for oncology," *IEEE Trans. Nucl. Sci.*, vol. 57, no. 1, pp. 246–255, Feb. 2010.

[23] S. Stute, S. Vauclin, H. Necib, N. Grotus, P. Tylski, N. Rehfeld, S. Hapdey, and I. Buvat, "Realistic and efficient modeling of radiotracer heterogeneity in Monte Carlo simulations of pet images with tumors," *IEEE Trans. Nucl. Sci.*, vol. 59, no. 1, pp. 113–122, Feb. 2012.

[24] B. M. Fuster, O. Esteban, X. Planes, P. Aguiar, C. Crespo, C. Falcon, G. Wollny, S. R. Sureda, X. Setoain, A. F. Frangi, M. J. Ledesma, A. Santos, J. Pavia, and D. Ros, "FocusDET, a new toolbox for siscom analysis. Evaluation of the registration accuracy using Monte Carlo simulation," *Neuroinformatics*, vol. 11, no. 1, pp. 77–89, 2013.

[25] Y. Zhang, M. Brady, and S. Smith, "Segmentation of brain MR images through a hidden Markov random field model and the expectation-maximization algorithm," *IEEE Trans. Med. Imag.*, vol. 20, no. 1, pp. 45–57, Jan. 2001.

[26] S. Smith, "Fast robust automated brain extraction," *Hum. Brain Mapp.*, vol. 17, no. 3, pp. 143–155, 2002.

[27] M. Jenkinson, C. Beckmann, T. Behrens, M. Woolrich, and S. Smith, "FSL," *NeuroImage*, vol. 62, no. 2, pp. 782–790, 2012.

[28] D. R. Haynor, R. L. Harrison, and T. K. Lewellen, "The use of importance sampling techniques to improve the efficiency of photon tracking in emission tomography simulations," *Med. Phys.*, vol. 18, no. 5, pp. 990–1001, 1991.

[29] K. Thielemans, C. Tsoumpas, S. Mustafovic, T. Beisel, P. Aguiar, N. Dikaios, and M. W. Jacobson, "STIR: Software for tomographic image reconstruction release 2," *Phys. Med. Biol.*, vol. 57, no. 4, pp. 867–883, 2012.

[30] N. Tzourio-Mazoyer, B. Landeau, D. Papathanassiou, F. Crivello, O. Etard, N. Delcroix, B. Mazoyer, and M. Joliot, "Automated anatomical labeling of activations in SPM using a macroscopic anatomical parcellation of the MNI MRI single-subject brain," *Neuroimage*, vol. 15, pp. 273–289, 2002.

[31] J. Ashburner, "A fast diffeomorphic image registration algorithm," *Neuroimage*, vol. 38, pp. 95–113, 2007.

[32] S. Stute, T. Carlier, K. Cristina, C. Noblet, A. Martineau, B. Hutton, L. Barnden, and I. Buvat, "Monte Carlo simulations of clinical PET and SPECT scans: Impact of the input data on the simulated images," *Phys. Med. Biol.*, vol. 56, no. 19, pp. 6441–6457, 2011.

[33] S. Stute, P. Tylski, N. Grotus, and I. Buvat, "Lucas: Efficient Monte Carlo simulations of highly realistic PET tumor images," in *IEEE Nucl. Sci. Symp. Conf. Rec.*, 2008, pp. 3285–3287.

[34] S. Jan, G. Santin, D. Strul, S. Staelens, K. Assie, D. Autret, S. Avner, R. Barbier, M. Bardies, P. M. Bloomfield, D. Brasse, V. Breton, P. Bruyndonckx, I. Buvat, A. F. Chatziioannou, Y. Choi, Y. H. Chung, C. Comtat, D. Donnarieix, L. Ferrer, S. J. Glick, C. J. Groiselle, D. Guez, P. F. Honore, S. Kerhoas-Cavata, A. S. Kirov, V. Kohli, M. Koole, M. Krieguer, D. J. van der Laan, F. Lamare, G. Largeron, C. Lartizien, D. Lazaro, M. C. Maas, L. Maigne, F. Mayet, F. Melot, C. Merheb, E. Pennacchio, J. Perez, U. Pietrzyk, F. R. Rannou, M. Rey, D. R. Schaart, C. R. Schmidtlein, L. Simon, T. Y. Song, J. M. Vieira, D. Visvikis, R. V. de Walle, E. Wieers, and C. Morel, "GATE: A simulation toolkit for PET and SPECT," *Phys. Med. Biol.*, vol. 49, no. 19, pp. 4543–4561, 2004.